Structural, Photoluminescence and Photoconductivity Properties of ZnO:Mn^{2+} Thin Films by Chemical Bath Deposition Method

N. Nithya[a,*] and S. Rugmini Radhakrishnan[b]

[a]*Department of Physics, Tamilnadu College of Engineering, Coimbatore – 641659, Tamilnadu, India.*
[b]*Department of Physics, Avinashilingam Institute for Home Science and Higher Education for Women, Coimbatore - 641043, Tamilnadu, India.*

Abstract

ZnO:Mn^{2+} thin films were deposited on glass substrate using chemical bath by alkalinity pH solution synthesis route. Mn^{2+} is varied between 0 and 10 mole% in steps of 2.5. The pure and Mn^{2+} doped ZnO nanocrystalline film have been compared structurally, morphologically and optically using, respectively, X-ray diffraction (XRD), scanning electron microscopy (SEM), transmission electron microscopy (TEM), UV–Vis. absorption studies photoluminescence (PL) and photoconductivity studies. The synthesized nanocrystalline films were composed of quantum dots with wurtzite structure. The UV–Vis absorption spectra revealed that pure and doped ZnO nanocrystalline film exhibit the blue shift in the absorption spectra with that of the bulk ZnO. The photoluminescence spectra showed enhanced luminescence intensity and the entry of Mn^{2+} into host lattice. Time resolved rise and decay photocurrent spectra are found to exhibit anomalous photoconductivity for pure and doped ZnO thin film wherein the photocurrent decreases even during steady illumination.

Key words:
Mn doped ZnO thin film, chemical bath deposition, TEM, UV-Vis., photoluminescence, photoconductivity

1. Introduction

A variety of manufactured metal oxide nanoparticles are being developed and incorporated into products where their unique catalytic capacity, optoelectronic properties and other characteristics make them attractive for a broad range of applications [1-3]. ZnO is one of the advanced optoelectronic materials which has been extensively investigated for its use in short wavelength optoelectronic devices such as light emitting diodes (LED) and laser diodes. Various thin film techniques have been used to synthesize doped ZnO, such as laser molecular-beam epitaxy [4], solid-state reactions [5-7] and pulsed laser deposition [8], but these methods always need high temperature and catalysts, which makes the synthesis procedure more complex and more expensive. Among these, chemical bath deposition technique is the most attractive one due to its perfect control of morphology, purity, crystallinity, composition and low cost for large-scale production. To modify structural, optical and other properties of ZnO nanostructures, it is practical to dope or decorate ZnO with other elements. Metal ion doped ZnO have also been reported, which include iron oxide (Fe_2O_3) [9], iron chloride ($FeCl_2$) [10], etc. In single-doped ZnO, Mn doped ZnO thin films have attracted most of the researchers' attention for their several advantages in terms of conductivity, thermal and chemical stability [11-12] while Cu^{2+} doped ZnO nanocrystalline films were reported elsewhere [13] for their enhancement of green band emission. Luminescence is one of the most distinguished features of doped ZnO samples [14–19]. The photoconductive aspects of ZnO can also take part in the accomplishment of some optoelectronic tasks such as transparent photoelectrodes [20], compound sensors [21-22] or in solar cell circuits [23]. Apparently, the study of the role related with optical and photoelectrical parameters that can take part in the use of ZnO nanocomposites looks to be motivating.

In the present work, we report the optical and photoconductivity properties of various concentrations (2.5, 5.0, 7.5 and 10.0 mole %) of Mn^{2+} doped with ZnO nanocrystalline films prepared by chemical bath deposition technique (CBD). The objective is to see if there is any change in behavior with the change in concentration of Mn^{2+} ions in host ZnO nanocrystalline films.

2. Experimental sections

2.1. Chemicals

Zinc acetate heptahydrate ($Zn(CH_3COO)_2.7H_2O$), urea ($CO(NH_2)_2$) and manganese chloride ($MnCl_2$) were purchased from Sigma-Aldrich. All the chemicals were of AR grade and used without further purification.

2.2. Sample preparation

1 mole $Zn(CH_3COO)_2.7H_2O$ and 2.5 mole % $MnCl_2$ were thoroughly mixed with 1 mole $CO(NH_2)_2$. Then the mixture was dissolved into 50 ml deionized water to get homogeneous mixture solution. The solution was continuously stirring for about 30 min. Few drops of NH_4OH solution were added into the mixture solution in order to maintain the pH at 9. The mixer solution was heated at 60 ºC with continuous stirring for about 70 minutes to produce ZnO:Mn^{2+} nanoparticles. The depositions take place on commercial glasses. These were cleaned with detergent in an ultrasonic cleaner and finally dried with N_2. The cleaned glass substrate was placed vertically inside the chemical bath containing solution. The bath was kept at room temperature (30 ºC) for 3 h. In order to maintain uniform thickness of the ZnO:Mn^{2+} thin film the coating time is maintained as 3 h. After the deposition, the substrate coated with film was taken out, washed with double distilled water and acetone, and then dried in hot oven at 60 ºC for an hour. The ZnO:Mn^{2+} thin film formation was started in about 10 min and completed within 180 min. The solution color was changed from whitish to greenish after deposition. Similar procedure was repeated for other Mn^{2+} doped (5.0, 7.5 and 10.0 mole %) ZnO thin films.

2.3. Instrumentation

The crystal structure of synthesized thin films was characterized by X-ray diffraction (PANalytical X-Pert Pro diffractometer with Cu Ka radiation (λ = 1.54056 Å) source over the diffraction angle 2θ between 20º and 80º). The film composition was determined by energy dispersive X-ray analyzer (EDX). Microstructural characterization at high magnifications was carried out using a transmission electron microscope (FEI Tecnai 30 G^2 300 kV, resolution 1.4 Å with 1 million magnification power). The absorption measurements were made by SHIMADZU UV-2400 PC spectrometer with a medium scan speed sampling interval 0.5 nm in the wavelength range 200-800 nm. The photoluminescence (PL) spectra were obtained on a FLUOROLOG-FL3-11 Spectroflorometer with wavelength resolution of 0.5 nm at room temperature. Xenon arc lamp of 450 W was used as the excitation light source. All the PL spectra in this study were acquired at an excitation wavelength of 300 nm. In photoconductivity study, an Hg bulb of 300 W was used as a photo-excitation source. The time-resolved rise and decay of photocurrent spectra are recorded using RISH Multi 15S with adapter RISH Multi SI-232. The observations have been made at room temperature in ambient air.

3. Results and discussion

3.1. Structural study

Fig. 1 shows the X-ray diffraction patterns (XRD) of ZnO:Mn^{2+} (0, 2.5, 5.0, 7.5 and 10.0 mole%) nanocrystalline films prepared by CBD technique. All the diffraction peaks can be indexed to the ZnO hexagonal phase [24]. The lattice constants are calculated for the most prominent peaks which are found to be close to standard values for the ZnO phase in the JCPDS date (JCPDS card no: 36-1451) [25].

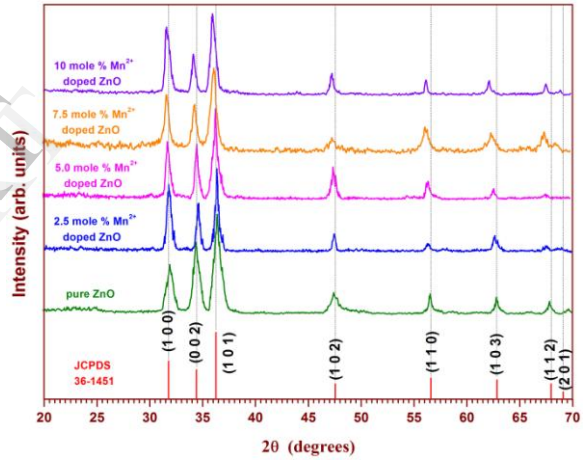

Figure 1: XRD patterns of ZnO:Mn^{2+} nanoparticles with different concentration of dopant (2.5, 5.0, 7.5 and 10.0 mole%)

The lattice parameters for the hexagonal wurtzite phase are calculated using formula [26]. The average crystallite size (D) of un-doped as well as Mn^{2+} doped ZnO thin films is estimated using Scherer's formula [27]. The estimated lattice parameters and average crystallite size of these nanoparticles is given in Table 1. No diffraction peak associated with Mn^{2+} related compounds is observed which may be due to low Mn^{2+} concentration. It is found that the variation in the lattice constants of Mn^{2+} doped ZnO nanoparticles are different as compared to that of un-doped ZnO nanoparticles which may be attributed to difference in ionic radii of Zn^{2+} (0.83 Å) and Mn^{2+} (0.91 Å).

The topographical analysis of as prepared pure and 10 mole% Mn^{2+} doped ZnO thin films were established

using transmission electron microscopic are shown in Fig. 2. The pure and doped nanoparticles show mono dispersity with less agglomeration. The average particles size inferred from the TEM micrographs is 10.2 nm for pure ZnO and 14.93 nm for 10.0 mole% Mn^{2+} doped ZnO thin films. The morphology of the particles is witnessed as spherical in shape.

Table 1: The observed structural data crystallite size from XRD measurements for pure and Mn^{2+}doped ZnO thin film. (*JCPDS file No. 36-1451)

Sample name	Dopant concentration	Calculated parameters			Crystal lite size
	mole %	a=b (Å)	c (Å)	Volume ($Å^3$)	nm
pure ZnO	–	3.2414 *3.2498	5.1887 *5.2066	47.212 *47.621	9.28
ZnO:Mn^{2+}	2.5	3.2684	5.2127	48.224	10.33
	5.0	3.2954	5.2589	49.459	11.89
	7.5	3.3147	5.3682	50.081	13.07
	10.0	3.2831	5.6091	52.359	15.28

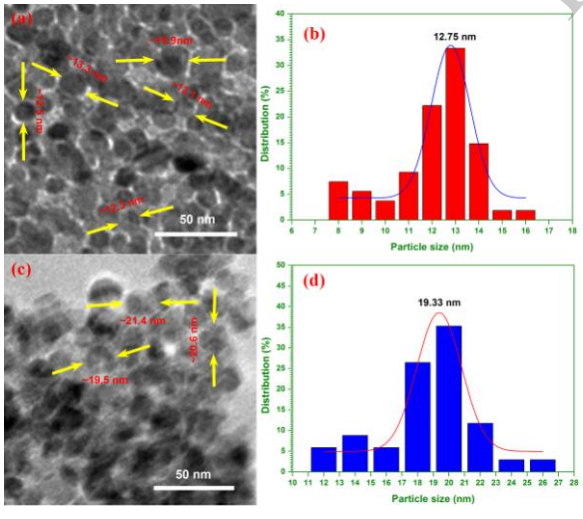

Figure 2: [a] TEM image of pure ZnO [b] particle size distribution histogram for pure ZnO [c] TEM image of 10.0 mole % Mn^{2+} doped ZnO [d] particle size distribution histogram for 10.0 mole % Mn^{2+} doped ZnO thin films

3.2. Optical absorption study

The optical absorption spectra of as prepared undoped ZnO and Mn (2.5, 5.0, 7.5 and 10 mole%) doped ZnO nanoparticles were recorded and shown in Fig. 3(a). The absorption data were analyzed and the band gap was estimated using the Tuac's relationship between the absorption coefficient (α) and the photon energy (hυ) [28]. The excitonic absorption peak for pure ZnO nanocrystalline file is observed at 341 nm. This is lower than the band gap wavelength of 388 nm for bulk ZnO [29]. Fig. 3(b) shows the plot of $(\alpha h\upsilon)^2$ *vs* $h\upsilon$ for pure ZnO and Mn^{2+} doped ZnO nanocrystalline films. The values of the direct bandgap energy (E_g) were obtained from the linear portion of the plots after extrapolating to zero as shown in Fig. 3(b). The obtained E_g values are 3.64, 3.51, 3.42, 3.36 and 3.30 eV for pure ZnO, 2.5 mole % Mn^{2+} doped ZnO, 5 mole % Mn^{2+} doped ZnO, 7.5 mole % Mn^{2+} doped ZnO and 10.0 mole % Mn^{2+} doped ZnO respectively. The E_g value shifted to the shorter (blue shift) or longer (red shift) wavelengths depending upon a number of factors. The shift to the shorter wavelength (blue shift) generally occurred when the particle size decreased [30]. When the particle size was smaller than the Bohr's radius, the blue shift can be explained by the size effect or the effect of quantum confinement [30]. The size of all the products in this experiment is beyond the Bohr's radius, thus the change in E_g values might be replacement of Zn^{2+} sites by the Mn^{2+} sites (dopant) in to the host ZnO lattices. The obtained energy gap values are in good agreement with ZnO nanoparticles [31]. As the concentration of Mn^{2+} increases in ZnO lattices, the optical bandgap energy decreases. This can be attributed to a decrease in the repulsion between the lowest conduction band edge of the ZnO that originated from the 4s state of the Zn atom and the highest valence band edge from the 2p state of the O atom [32].

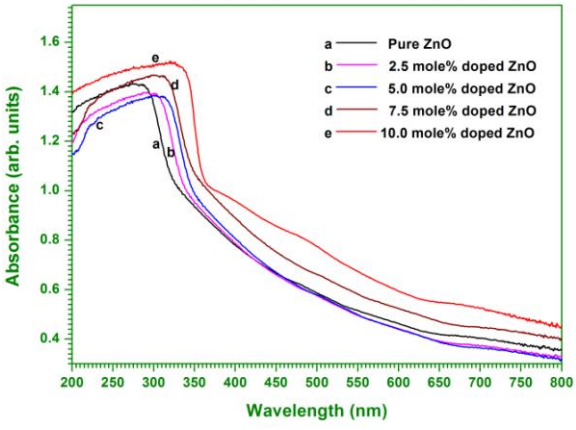

Figure 3(a): UV-Vis. absorption spectra of pure and different concentration of Mn^{2+} doped ZnO nanocrystalline films

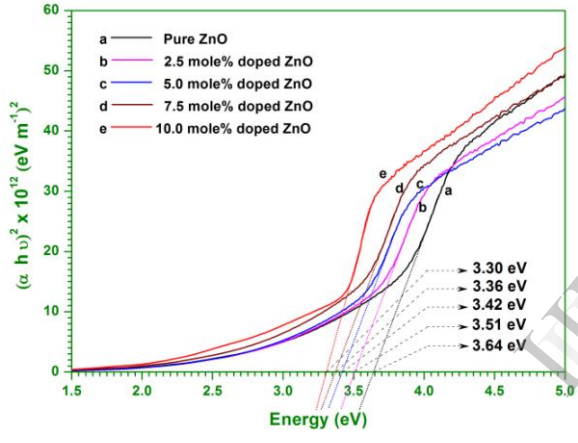

Figure 3(b): Optical bandgap measurements of pure and different concentration of Mn^{2+} doped ZnO nanocrystalline films

3.3. Photoluminescence study

Photoluminescence (PL) study is a powerful method for investigating the effects of impurity doping on optical properties of semiconductor nanostructures with direct band gap, because doped nanostructures are expected to have different optical properties compare to undoped nanostructures. Fig. 4 shows the PL spectra's of pure and doped ZnO nanostructures on glass substrate.

All the as synthesized samples shows the existence of two peaks, a narrow ultra-violet (UV) emission peak centered at 350 nm (3.54 eV) and a broad visible light emission extending from approximately 480 nm to 680 nm with a strong defect emission peak. The visible band emission corresponds to the singly ionized oxygen vacancy in ZnO. This emission results from the recombination of a photo-generated hole with the singly ionized charge state of the specific defect. Compared to Mn doped ZnO thin film, the high intensity of the green emission of ZnO nanocrystalline particles may be due to the high density of oxygen vacancies during the preparation. Whereas, the narrow UV emission intensity indicates that the synthesized film possess perfect crystallinity [33].

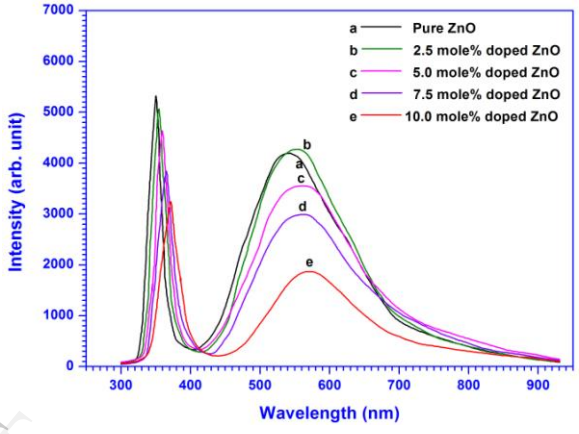

Figure 4: Photoluminescence spectra of pure and different concentration of Mn^{2+} doped ZnO thin films.

All the as synthesized samples shows the existence of two peaks, a narrow ultra-violet (UV) emission peak centered at 350 nm (3.54 eV) and a broad visible light emission extending from approximately 480 nm to 680 nm with a strong defect emission peak. The visible band emission corresponds to the singly ionized oxygen vacancy in ZnO. This emission results from the recombination of a photo-generated hole with the singly ionized charge state of the specific defect. Compared to Mn doped ZnO thin film, the high intensity of the green emission of ZnO nanocrystalline particles may be due to the high density of oxygen vacancies during the preparation. Whereas, the narrow UV emission intensity indicates that the synthesized film possess perfect crystallinity [33].

3.4. Photoconductivity study

The variation of field dependence dark current (I_d) and photocurrent (I_p) with applied voltage (V) for pure and doped ZnO nanocrystalline films for different concentrations of Mn^{2+} ions are shown in Fig. 5(a-b). The corresponding variation in ln – ln scale is shown Fig. 5(c-d). It is observed that both dark and photo currents of pure and Mn^{2+} doped ZnO nanocrystalline films increase linearly with the applied voltage. The photocurrent of both pure and doped ZnO

nanocrystalline film is more than the dark current, which is termed as positive photoconductivity. All the synthesized pure and Mn^{2+} doped ZnO nanocrystalline films considered in the present study are found to exhibit positive photoconductivity. This may be attributed to the generation of mobile charge carriers caused by absorption of photons [34]. It is also observed that, the photocurrent of lower concentration (2.5 and 5.0 mole %) of Mn^{2+} doped ZnO nanocrystalline films are higher than that of pure ZnO. However at the higher concentration (7.5 and 10.0 mole %) the behavior is lesser than that of pure ZnO. The variation of dark-current and photocurrent with different dopant concentrations (mole %) of Mn^{2+} doped ZnO at constant applied voltage (30 V) is shown in Fig. 6. Form the Fig. 6 we observed that the ZnO doped with 5.0 mole% Mn^{2+} is more photosensitive as compared to other Mn^{2+} doped ZnO nanocrystalline films. The variation of dark-current ($\ln(I_d)$) with the applied voltage ($\ln(V)$) is found to be linear (r = 1) for un-doped as well as lower concentration (2.5 and 5.0 mole %) of Mn^{2+} doped ZnO nanocrystalline film whereas at higher concentrations (7.5 and 10.0 mole %) the behavior is super-linear (r > 1). However, from the plots $\ln(I_p)$ *vs* $\ln(V)$ (see Fig. 5(c-d) are found to be super-linear for un-doped as well as Mn^{2+} doped ZnO nanocrystalline films with different concentrations considered in the present study. Super-linear behavior suggests that extra carriers are injected into the nanocrystalline film from the electrode side [35].

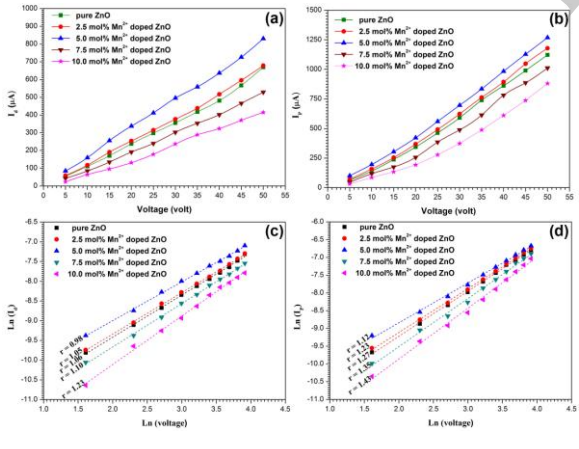

Figure 5: (a) Variation of dark current (b) variation of photo current (c) variation of $\ln(I_d)$ vs $\ln(V)$ (d) variation of $\ln(I_p)$ vs $\ln(V)$ with applied voltage of pure and different concentration of Mn^{2+} doped ZnO thin films

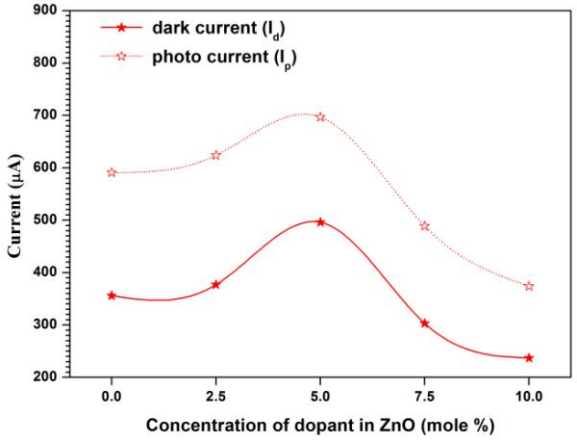

Figure 6: The variation of dark and photo current with different concentrations (mole %) of Mn^{2+} doped ZnO at constant applied voltage (30 V)

After attaining maximum value of photocurrent it start decaying (anomalous behavior of photocurrent) even during steady illumination. This is caused by the presence of imperfection centers in the forbidden gap [35] of the nanocrystalline films. Also the anomalous behavior of photocurrent may be attributed to dominance of the process of photo-induced adsorption of oxygen molecules [39]. Adsorption of oxygen molecules captures free carriers, which results in reduction in photocurrent. The anomalous behavior of photocurrent may also be attributed to the variation of the surface depletion region [40]. Bera and Basak [37] have reported the similar anomalous behavior in ZnO nanowire. After that, the photocurrent decreases exponentially during steady illumination for a long while and attains a constant value. When illumination is switched off, the photocurrent further decreases exponentially and attains a constant value for long time. This is due to the electrons recombine with holes and is captured by re-adsorbed oxygen molecules [41]. The photocurrent rise and decay curves are also governed by trap levels and recombination centers lying in the forbidden region of the photoconductor, so these curves are used to know the nature and distribution of traps and recombination centers [42]. As the concentration of Mn^{2+} increases (2.5 and 5.0 mole %) more defect states are introduced in the host ZnO which contributing more photocurrent. Further the concentration of Mn^{2+} increases (7.5 and 10.0 mole %) the photocurrent decreases due to Mn–Mn interaction. The concentrations of defect states are supposed to get reduce the photocurrent [43]. In our present study, even the small amount of dopants in the host ZnO lattices highly enhances the photocurrent. The rise and decay of photocurrent of the ZnO nanocrystalline film is highly

changed with the change in concentration of dopants in the host ZnO nanocrystalline film.

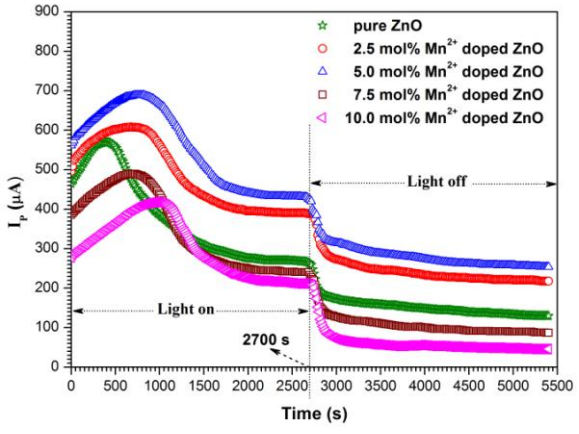

Figure 7: Variation of time resolved rise and decay of photocurrent spectra of pure and different concentration of Mn^{2+} doped ZnO thin films.

4. Conclusion

Pure and Mn^{2+} doped ZnO thin films are successfully prepared by chemical bath deposition technique. The structural and morphological studies were studied. XRD analysis confirms the prepared nanocrystalline films are in wurtzite structure and the average crystallite size for pure ZnO is 9.28 nm. TEM and EDS analysis shows the particles are in spherical shape and the presence of dopant in the ZnO system. UV–visible spectra show the free exciton absorption band and gets red shifted with increasing concentration of Mn^{2+} in ZnO lattices. The PL analysis shows the existence of both UV and visible emissions. Also it shows red-shift and decrease in visible emission with Mn^{2+} doping in ZnO host lattices. Un-doped as well Mn^{2+} doped ZnO nanoparticles are found to exhibit an anomalous photoconductivity which may be attributed to photodesorption of water molecules.

Acknowledgments

The authors would like to thank Dr. S. Rajagopal for their contributions to the field of semiconductor nanoparticles and many discussions and exchange of ideas and support. We are also grateful to Dr. D. Pukazhselvan, Padova University, for helpful characterization and discussions support.

References

[1] Z.L. Wang, (2004) *Journal of Physics: Condensed Matter* **16**, R829-R858.

[2] N.S. Hussain, P.J. Cardoso,G. Hungerford, M.J.M. Gomes, Nasar Ali, J.D. Santos, S. Buddhudu, (2009) *J. Nanosci. Nanotechnol.* **9**, 3555.

[3] Y. Mai, A. Watanabe (2004) *J. Mater. Sci.: Mater. Electron.* **15**, 743.

[4] D. C. Look, D. C. Reynolds, C. W. Litton, R. L. Jones, D. B. Eason and G. Cantwell (2002) *Appl. Phys. Lett.* **81**, 1830

[5] C. Jin, X. Yuan, W. Ge, J. Hong and X. Xin (2003) *Nanotechnology* **14,** 667

[6] K. Lib, H. Luoc, T. Ying, (2011) *Materials Science in Semiconductor Processing*, **14**, 184–187

[7] Y. Zhu, Y. Zhou, (2008) *Applied Physics A,* **92**, 275-278

[8] A.Ohtomo and A.Tsukazaki (2005) *Semicond. Sci. Technol.* **20**, S1

[9] B. Panigrahy, M. Aslam and D. Bahadur, (2012) *Nanotechnology* **23**, 115601.

[10] T. M. Hammad, S. Griesing, M. Wotocek, S. Kuhn, R. Hempelmann, U. Hartmann, J. K. Salem (2013) *Int. J. of Nanoparticles*, **6**, 324 - 337

[11] I. Sameera, R. Bhatia, V. Prasad (2010) *Physica B: Condensed Matter* **405**, 1709–1714

[12] L. Zhao, J. Zhang, S. Sun (2012) *Journal of Luminescence* **132**, 2595–2598

[13] N. Nithya, S. Rugmini Radhakrishnan, (2013) *International Journal of Physical, Chemical & Mathematical Sciences*, **2**, 45-54.

[14] X.Liu, X.Wu ,H.Cao, R.P.H.Chang, (2004) *J. Appl. Phys.* **95**, 3141.

[15] M. Yin, Y.Gu, I.L.Kuskovsky, T. Andelman, Y.Zhu, G.F.Neumark, S. O'Brien, (2004) *J. Am. Chem. Soc.* **126**, 6206.

[16] S.A.Studenikin, N.Golego, (1998) *J. Appl. Phys.* **84**, 2287.

[17] B.Lin, Z.Fu, Y.Jia, (2001) *Appl. Phys. Lett.* **79**, 943.

[18] D. Banerjee, J.Y.Lao, D.Z.Wang, J.Y.Huang, Z.F.Ren, D.Steeves, B.Kimball, M. Sennett, (2003) *Appl. Phys. Lett.* **83**, 2061.

[19] T.-B.Hur, G.S.Jeen, Y.-H.Hwang, H.-K.Kim, (2003) *J. Appl. Phys.* **94**, 5787.

[20] U. Ozgur, Ya. I. Alivov, C. Liu, A. Teke, M.A. Reshchikov, S.Dogan, V. Avrutin, S.-J. Cho, H. Morkoc, (2005) *J. Appl. Phys.* **98**, 041301–103.

[21] L. Castaneda, O.G. Morales-Saavedra, D.R. Acosta, A. Maldonado, M. de la, L. Olvera, (2006) *Phys. Status Solidi (a)* **203**, 1971.
[22] H.-J.Lee, S.-Y.Jeong, J.-Y. Hwang, C.R. Cho, (2003) *Europhys. Lett.* **64**, 797.
[23] H. Liang, R.G. Gordon, (2007) *J. Mater. Sci.* **42**, 6388.
[24] A. Umar and Y B Hahn (2006) *Nanotechnology* **17**, 2174
[25] G. Shen, Y. Bando and C. J. Lee (2005) *J. Phys. Chem. B*, **109**, 10578–10583
[26] R. Yogamalara, R. Srinivasana, A. Vinub, K. Arigab, A. C. Bose (2009) *Solid State Communications* **149**, 1919–1923
[27] B.D. Culty, (1978) Elements of X-ray Diffraction, Addision-Wesley, New York.
[28] J. Tauc, R. Grigorovici, A.Vancu, (1966) *Phys. Status Solidi b* **15**, 627–637.
[29] P. Kumbhakar, D. Singh, C. S. Tiwary, A. K. Mitra, (2008) *Chalcogenide Lett.* **5**, 387–394.
[30] S. Suwanboon, P. Amornpitoksuk, A. Haidoux, J.C. Tedenac, (2008) Journal of Alloys and Compounds **462**, 335–339
[31] K.F. Lin, H.M. Cheng, H.C. Hsu, L.J. Lin, W.F. Hsieh, (2005) *Chemical Physics Letters* **409**, 208–211
[32] P. Amornpitoksuk, S. Suwanboon, S. Sangkanu, A. Sukhoom, N. Muensit, (2012) *Superlattices and Microstructures* **51**, 103–113.
[33] S. Maensiri, C. Masingboon, V. Promarak, S. Seraphin, (2007) *Optik. Mater.* **29**, 1700–1705.
[34] V.N. Joshi (1990), 'Photoconductivity', Marcel Dekker, New York
[35] S. Devi and S.G. Prakash (1993) *Ind. J. Pure Appl. Phys.* **31**, 161–165.
[36] S. E. Ahn, H. J. Ji, K. Kim, G. T. Kim, C. H. Bae, S. M. Park, Y. K. Kim, J. S. Ha, (2007) *Appl. Phys.Lett.* **90**, 153106.
[37] A. Bera and D. Basak, (2009) *Appl. Phys. Lett.* **94**, 163119.
[38] L. Peng, J.-L. Zhai, D.-J. Wang, P. Wang, Y. Zhang, S. Pang, T.-F. Xie, (2008) *Chem. Phys. Lett.* **456**, 231.
[39] A. Bera and D. Basak, (2009) *Appl. Mater. Inter.* **1**, 2066.
[40] Z.-M. Liao, H.-Z. Zhang, D.-P. Yu, (2010) *Appl. Phys. Lett.* **97**, 033113.
[41] X.G. Zheng, Sh Q. Li, W. Hu, D. Chen, N. Zhang, M.J. Shi, J.J. Wang,. Zhang Ch L, (2007) *J. Lumin.* **122**, 198.
[42] J.F. Randall, J.H.F. Wilkins, (1945) *Proc. R. Soc. A* **184**, 366.
[43] S. Taguchi, A. Ishizumi, T. Tayagaki, Y. Kanemitsu, (2009) *Appl. Phys. Lett.* **94**, 173101.